



Original article

3D-QSAR studies on the inhibitors of AP-1 and NF- κ B mediated transcriptional activationJin Qin^a, Huanxiang Liu^b, Jiazhong Li^a, Yueying Ren^a, Xiaojun Yao^{*,a}, Mancang Liu^a^a Department of Chemistry, Lanzhou University, Lanzhou 730000, China^b School of Pharmacy, Lanzhou University, Lanzhou 730000, China

ARTICLE INFO

Article history:

Received 26 January 2008

Received in revised form

4 December 2008

Accepted 8 December 2008

Available online 16 December 2008

Keywords:

3D-QSAR

AP-1

NF- κ B

Transcriptional activation

Anti-inflammatory

ABSTRACT

Comparative molecular field analysis (CoMFA) and comparative molecular similarity indices analysis (CoMSIA) were performed on a series of 68 inhibitors of AP-1 and NF- κ B mediated transcriptional activations. The CoMFA model produced statistically significant results with the cross-validated q^2 of 0.594 and the conventional correlation coefficient r^2 of 0.968. The best CoMSIA model was obtained by the combination use of steric, electrostatic, hydrogen-bond donor and acceptor fields. The corresponding q^2 and r^2 of CoMSIA model were 0.703 and 0.932, respectively. From the cross-validated results, it can be seen that the CoMSIA model has a better predictive ability than CoMFA model due to the importance of the hydrogen bonds for the activity of these inhibitors. The predictive abilities of the two models were further validated by a test set of 15 compounds. The models gave predicted correlation coefficient r^2_{pred} of 0.891 for CoMFA model and 0.810 for CoMSIA model. Based on the above results, we identified the key structural features that may help to design potent inhibitors with improved activities: (1) the NH linker at the position R₄ acts as important hydrogen-bond donor and any group on phenyl or 2-thienyl ring of R₁ substituent decreases inhibitory activity, (2) further structural modification of compound **50** on the phenyl ring of the quinazoline ring considering steric, electrostatic and hydrogen-bond acceptor properties will influence the inhibitory activity.

© 2009 Elsevier Masson SAS. All rights reserved.

1. Introduction

In certain autoimmune diseases and chronic inflammatory states, the continuous activation of T-lymphocytes (T-cells) leads to a self-perpetuating destruction of normal tissues or organs [1]. This activation initiates a cascade of events that result in the over-production of certain transcription factors [2] and proinflammatory cytokines [3,4]. Two important transcription factors, nuclear factor- κ binding (NF- κ B) and activator protein-1 (AP-1), control the production of many cytokines and are relevant to immunoinflammatory diseases [5–8]. Therefore, modulation of either one or both of these transcription factors should lead to suppression of cytokine levels and represent attractive targets for the prevention of immunoinflammatory diseases [9]. As these two transcription factors are regulated by distinct signaling pathway involving several proteins, many key factors involved in their activation pathway can be the targets for drug design [10]. There are many reports about inhibitors of NF- κ B or AP-1 transcriptional activation [11–17], but very few compounds are known to inhibit both the

AP-1 and NF- κ B mediated transcriptional activation [10]. Recently, Palanki et al. designed a series of novel compounds (Table 1) and tested their activity in the transfected human Jurkat T-cells [18–22]. These compounds could interfere with cyclosporin-resistant CD28 co-stimulation as well as CD3-mediated signaling pathway [10], which were required both for the transcriptional activation of AP-1 and NF- κ B [23]. In order to design more compounds with desired activity, it is very necessary and useful to investigate the quantitative structure–activity relationships (QSARs) of these known inhibitors that can both inhibit the transcriptional activation of AP-1 and NF- κ B.

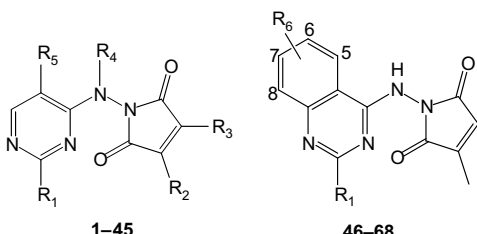
Nowadays, three-dimensional quantitative structure–activity relationship (3D-QSAR) approaches, such as comparative molecular field analysis (CoMFA) [24] and comparative molecular similarity analysis (CoMSIA) [25,26] have been widely used in drug design [27–29]. The contour maps obtained from these models could not only help us to understand the quantitative relationship between the molecular structures and their activity but also can help to design new potent inhibitors with desired activity. In this work, 3D-QSAR models were built based on a series inhibitors of AP-1 and NF- κ B mediated transcriptional activation [22,23] using CoMFA and CoMSIA methods.

* Corresponding author. Tel.: +86 931 891 2578; fax: +86 931 891 2582.

E-mail address: xjyao@lzu.edu.cn (X. Yao).

Table 1

Structures and biological activities of the compounds used in training and test sets.



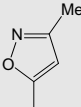
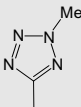
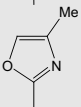
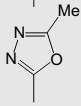
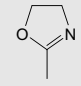
Compound	R ₁	R ₂	R ₃	R ₄	R ₅	R ₆	pIC ₅₀
1 ^a	CF ₃	Me	H	H	CO ₂ Et		6.000
2	Me	Me	H	H	CO ₂ Et		4.796
3	Et	Me	H	H	CO ₂ Et		5.000
4 ^a	<i>t</i> -Bu	Me	H	H	CO ₂ Et		6.000
5	SMe	Me	H	H	CO ₂ Et		6.699
6	Phenyl	Me	H	H	CO ₂ Et		7.000
7	2-Thienyl	Me	H	H	CO ₂ Et		7.699
8 ^a	4-Pyridyl	Me	H	H	CO ₂ Et		5.222
9	2,6-Dichloro-4-Pyridyl	Me	H	H	CO ₂ Et		5.699
10	3-Quinoliny	Me	H	H	CO ₂ Et		5.222
11	4-(2-Methyl)-thiazolyl	Me	H	H	CO ₂ Et		5.097
12	1-(3,5-Dimethyl)-pyrazolyl	Me	H	H	CO ₂ Et		5.000
13 ^a	4-Methoxy-phenyl	Me	H	H	CO ₂ Et		6.046
14	3-Methoxy-phenyl	Me	H	H	CO ₂ Et		5.301
15	4-Fluoro-phenyl	Me	H	H	CO ₂ Et		6.155
16 ^a	4-Chloro-phenyl	Me	H	H	CO ₂ Et		6.523
17	4-Trifluoro-methyl-phenyl	Me	H	H	CO ₂ Et		6.398
18 ^a	3-Bromo-phenyl	Me	H	H	CO ₂ Et		6.155
19	3-Nitro-phenyl	Me	H	H	CO ₂ Et		5.155
20	3-Thienyl	Me	H	H	CO ₂ Et		7.000
21 ^a	5-Methyl-2-thienyl	Me	H	H	CO ₂ Et		6.699
22	5-Chloro-2-thienyl	Me	H	H	CO ₂ Et		6.523
23	2-Benzo-thienyl	Me	H	H	CO ₂ Et		5.398
24	2-Furanoyl	Me	H	H	CO ₂ Et		6.699
25	Cyclopropyl	Me	H	H	CO ₂ Et		6.000
26	2-(Cyclo-hex-2-enyl-methyl)	Me	H	H	CO ₂ Et		5.699
27	3,5-Dichloro-phenyl	Me	H	H	CO ₂ Et		6.523
28 ^a	Benzyl	Me	H	H	CO ₂ Et		5.155
29	Phenoxy	Me	H	H	CO ₂ Et		4.824
30	2-Phenyl-thio	Me	H	H	CO ₂ Et		6.000
31	2-Phenyl-sulfonyl	Me	H	H	CO ₂ Et		5.000
32	Phenyl	Me	H	Me	CO ₂ Et		5.699
33 ^a	Phenyl	Me	H	Ac	CO ₂ Et		5.398
34	2-Thienyl	Me	H	Me	CO ₂ Et		6.000
35	4-Fluoro-phenyl	Me	H	Me	CO ₂ Et		5.523
36	Et	Me	H	Me	CO ₂ Et		5.000
37	CF ₃	Me	Me	H	CO ₂ Et		5.000
38	CF ₃	Phenyl	H	H	CO ₂ Et		4.699
39 ^a	CF ₃	H	H	H	CO ₂ Et		5.000
40	2-Thienyl	Me	H	H			6.523
41	2-Thienyl	Me	H	H	CN		5.301
42	2-Thienyl	Me	H	H			6.699
43 ^a	2-Thienyl	Me	H	H			6.699
44	2-Thienyl	Me	H	H			6.523

Table 1 (continued)

Compound	R ₁	R ₂	R ₃	R ₄	R ₅	R ₆	pIC ₅₀
45	2-Thienyl	Me	H	H			6.699
46	2-Thienyl						7.222
47	Phenyl						7.000
48 ^a	CF ₃						7.000
49	2-Thienyl					5-OMe	8.097
50	2-Thienyl					6-OMe	8.523
51 ^a	2-Thienyl					7-OMe	7.699
52	2-Thienyl					8-OMe	7.301
53	2-Thienyl					6,7-Di-OMe	7.301
54	2-Thienyl					6,7,8-Tri-OMe	7.398
55	2-Thienyl					5-F	7.301
56	2-Thienyl					6-Cl	7.699
57 ^a	2-Thienyl					5-Me	7.699
58	2-Thienyl					7-(N-morpholyl)	6.699
59	2-Thienyl					7-(NMe ₂)	7.398
60	CF ₃					5-OMe	8.000
61	CF ₃					6-OMe	7.523
62	CF ₃					5-Me	6.398
63	CF ₃					6-SMe	7.097
64	CF ₃					6-SOMe	6.000
65	CF ₃					6-SO ₂ Me	5.046
66	CF ₃					6-OH	7.000
67 ^a	CF ₃					7-(1-Piperidyl)	6.699
68	CF ₃					7-(NMe ₂)	7.699

^a Test set compound.

2. Materials and methods

2.1. Data sets

In this study, the involved 68 compounds were taken from the works of Palanki et al. [22,23] and their structures were listed in Table 1. The in vitro inhibitory activity (IC₅₀) was transformed to negative logarithmic units marked as pIC₅₀ in the CoMFA and CoMSIA analysis. The data set was divided into a training set (53 compounds) to generate the 3D-QSAR models and a test set (the rest 15 compounds) to evaluate the predictive ability of the developed models (shown in Table 1). In addition, the compounds in the test set were considered to cover the wide range of the activity in the whole data set (Fig. 1).

2.2. Molecular modeling and alignment

Molecular modeling and statistical analysis were performed using the molecular modeling package SYBYL 6.9 [30]. Energy minimization of the molecular structure was performed using the Powell gradient algorithm with the Tripos force field [31] and Gasteiger–Hückel charge [32]. The lowest energy conformation was used to perform 3D-QSAR calculations.

Because the bioactive conformations of these inhibitors were not known, the most potent compound **50** was chosen as the template for alignment. The reference atoms in the compound **50** for alignment are shown in Fig. 2A. Each compound was aligned to the template using the Align Database function due to its easy implementation and effectiveness. The aligned compounds are displayed in Fig. 2B.

2.3. CoMFA and CoMSIA models

The CoMFA descriptors, steric (Lennard–Jones 6–12 potential) and electrostatic (Coulomb potential) fields energies between the probe

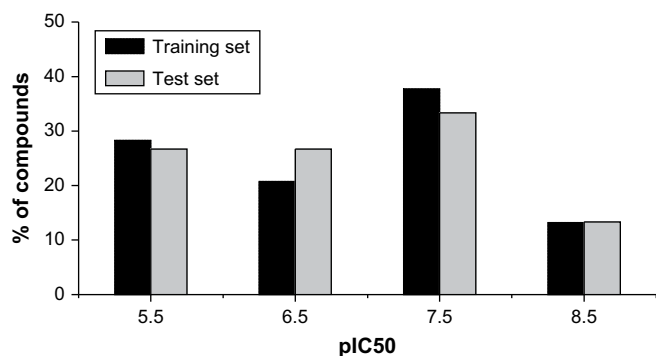


Fig. 1. Distribution of the inhibitory activities for training set and test set compounds.

and the test molecule at each lattice intersection were calculated with a grid step size of 2 Å using sp^3 C⁺ as probe atom. The CoMFA fields generated automatically were scaled by the CoMFA-STD method with default energy of 30 kcal/mol.

In the case of CoMSIA models, similarity indices' descriptors were derived according to the method developed by Klebe et al. [25,26] with the same lattice box used in the CoMFA calculations. Five fields, i.e. steric, electrostatic, hydrophobic, hydrogen-bond

donor and hydrogen-bond acceptor fields were evaluated using the same probe atom as CoMFA analysis. In general, CoMSIA similarity indices (A_F) for a molecule j with atoms i at a grid point q was calculated as:

$$A_{F,K}^q(j) = - \sum_{i=1}^n \omega_{\text{probe},k} \omega_{ik} e^{-\alpha r_{iq}^2} \quad (1)$$

where ω_{ik} is the actual value of physicochemical property k of atom i ; $\omega_{\text{probe},k}$ is the value of the probe atom, α is the attenuation factor and the default value of 0.3 was used. In CoMSIA, the steric indices are related to the third power of the atomic radii, the electrostatic descriptors are derived from partial atomic charges, and the hydrophobic fields are derived from atom based parameters [33]. The hydrogen-bond donor and acceptor atoms within a putative protein environment are derived from experimental values [34,35].

2.4. Regression analysis

The partial least squares (PLS) [36,37] method implemented in the QSAR module of SYBYL was used to construct and validate the models. The CoMFA/CoMSIA descriptors derived above and pIC₅₀ values were used as dependent variable in PLS regression analysis. The performance of models was calculated using the leave-one-out (LOO) cross-validation method [24,38]. The cross-validated coefficient, q^2 , was evaluated as:

$$q^2 = 1 - \frac{\sum_{i=1}^n (Y_{\text{predicted}} - Y_{\text{observed}})^2}{\sum_{i=1}^n (Y_{\text{observed}} - Y_{\text{mean}})^2} \quad (2)$$

where $Y_{\text{predicted}}$, Y_{observed} , and Y_{mean} are predicted, observed, and mean values of the target property (pIC₅₀), respectively. The optimal number of components (ONC) equal to that yielding the highest cross-validated q^2 was used to generate the final PLS regression (non-cross-validated conventional analysis) models. The conventional correlation coefficient r^2 and its standard error of estimate (SEE) were subsequently computed for the final PLS models. CoMFA and CoMSIA coefficient maps were generated by interpolation of the pairwise products between the PLS coefficients and the standard deviations of the corresponding CoMFA or CoMSIA descriptor values.

3. Results and discussion

3.1. CoMFA and CoMSIA statistical results

Several different CoMFA and CoMSIA models were developed and the final models were selected according to the statistically significant parameters. The statistical results for CoMFA and CoMSIA models are summarized in Table 2. The best CoMFA model gave the cross-validated q^2 of 0.594 with an optimal number of components (ONC) of 6 and non-cross-validated correlation coefficient r^2 of 0.968.

In CoMSIA analysis, the five different descriptor fields are not totally independent of each other and such dependencies on individual fields usually decrease the statistical significance of the CoMSIA models [26,39]. Some possible combinations of different fields were performed to determine the best CoMSIA model (Table 3). The steric, electrostatic and H-bond acceptor fields yielded the best individual field model with cross-validated q^2 of 0.615, 0.585 and 0.509, respectively. The highest cross-validated q^2 was obtained by using the combination of steric, electrostatic, H-bond acceptor and donor fields ($q^2=0.703$, $r^2=0.932$). The corresponding model was selected for the further analysis and for the

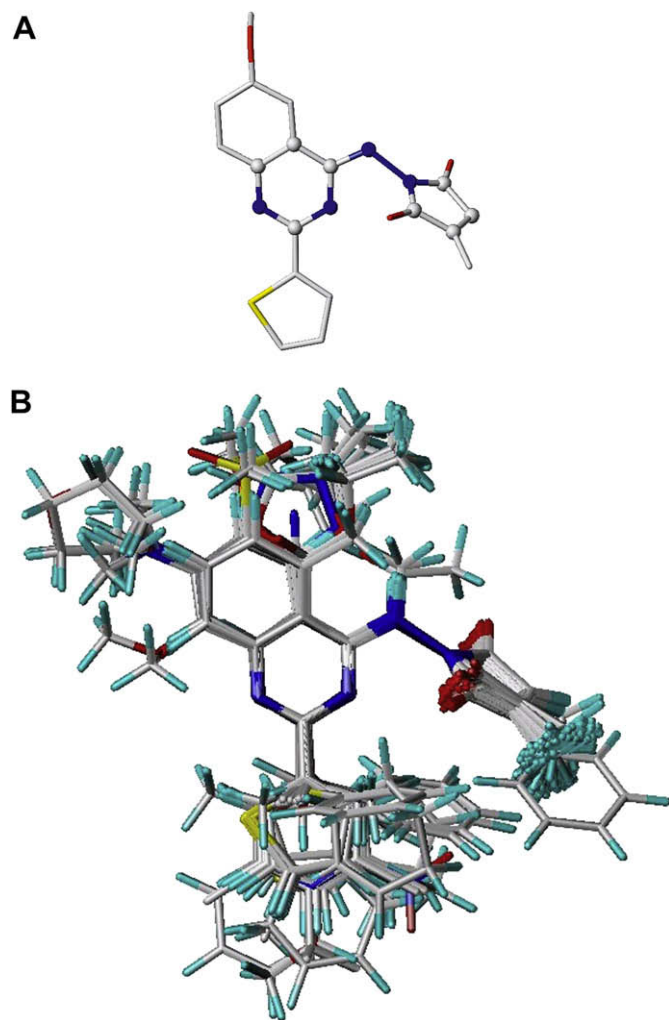


Fig. 2. Alignment of all the molecules in training and test sets: (A) scaffold of compound 50, the atoms used for alignment are depicted as balls; (B) 3D-view of aligned molecules.

Table 2Summary of CoMFA and CoMSIA results^a.

	CoMFA	CoMSIA
q^2 ^b	0.594	0.703
ONC ^c	6	6
r^2 ^d	0.968	0.932
SEE ^e	0.194	0.282
F_{test} ^f	232.513	105.730
r^2_{pred} ^g	0.891	0.810
S	0.566	0.210
E	0.434	0.406
D	–	0.148
A	–	0.236

^a Abbreviations: S (steric); E (electrostatic); H (hydrophobic); D (H-bond donor); A (H-bond acceptor).

^b Cross-validated correlation coefficient after leave-one-out procedure.

^c Optimal number of principal components.

^d Correlation coefficient.

^e Standard error of estimate.

^f Ratio of r^2 explained to unexplained = $r^2/(1 - r^2)$.

^g Predicted correlation coefficient for test set of compounds.

prediction of the test set compounds. From the cross-validation results, it can be seen that the CoMSIA model has a better predictive ability than CoMFA model due to the importance of the hydrogen bonds for the activity of these inhibitors.

When the CoMFA and CoMSIA models were applied to the 15 test compounds, both models gave satisfactory results. The corresponding correlation coefficient r^2_{pred} of the CoMFA and CoMSIA models for the test set were 0.891 and 0.810, respectively. The average residual values of the two models were 0.013 and 0.085. The population variances (RSS/ n) for residuals of the two models were 0.091 and 0.134, respectively. The details of predicted pIC₅₀ values and the corresponding residuals based on the best models are listed in Table 4. The plot of the predicted versus observed pIC₅₀ values for the two models are shown in Fig. 3.

3.2. CoMFA contour maps

The steric and electrostatic contour maps of the best CoMFA model are shown in Fig. 4. Compounds **6** and **50** were used as the reference molecules for compounds **1–45** and **46–68**, respectively. The green contours (80% contribution) represent regions where bulky substituents would increase the inhibitory activity, while the yellow contours (20% contribution) represent regions where steric bulky group would be unfavourable. Furthermore, the blue and red contours (80% and 20% contributions) depict the position where positively charged groups and negatively charged groups would be favorable, respectively.

Table 3

Combination of different CoMSIA fields and their results.

Fields ^a	q^2	ONC	r^2	SEE	F_{test}	Contribution				
						S	E	H	D	A
S	0.615	6	0.907	0.330	74.878	1.00	–	–	–	–
E	0.585	4	0.804	0.469	49.348	–	1.00	–	–	–
H	0.383	1	0.462	0.755	43.848	–	–	1.00	–	–
D	0.207	1	0.273	0.878	19.160	–	–	–	1.00	–
A	0.509	2	0.639	0.625	44.237	–	–	–	–	1.00
SEHD	0.621	6	0.916	0.314	85.953	0.163	0.424	0.298	0.115	–
SEHA	0.676	6	0.934	0.279	108.255	0.152	0.354	0.314	–	0.179
SEDA	0.703	6	0.932	0.282	105.730	0.210	0.406	–	0.148	0.236
SHDA	0.434	3	0.678	0.596	34.394	0.163	–	0.406	0.134	0.297
EHDA	0.668	6	0.912	0.322	79.508	–	0.373	0.298	0.114	0.215
SEHDA	0.676	6	0.929	0.290	99.837	0.135	0.317	0.243	0.118	0.188

^a Abbreviations: S (steric); E (electrostatic); H (hydrophobic); D (H-bond donor); A (H-bond acceptor).

In the CoMFA steric contour map (Fig. 4A), the steric favorable green contour on 2-thienyl (compound **6**) and phenyl (compound **50**) rings at 2-position of pyrimidine ring indicates that bulky group in this region is important for inhibitory activity. By

Table 4

Observed and predicted activities for training and test sets' compounds by 3D-QSAR models.

Compound	Observed pIC ₅₀	CoMFA		CoMSIA	
		Predicted	Residual	Predicted	Residual
Training set					
2	4.796	4.607	−0.189	4.933	0.137
3	5.000	5.134	0.134	4.914	−0.086
5	6.699	6.339	−0.360	6.449	−0.250
6	7.000	6.629	−0.371	6.281	−0.719
7	7.699	7.667	−0.032	7.782	0.083
9	5.699	5.971	0.272	5.764	0.065
10	5.222	5.095	−0.127	5.029	−0.193
11	5.097	5.340	0.243	5.449	0.353
12	5.000	5.057	0.057	4.892	−0.108
14	5.301	5.162	−0.139	5.501	0.200
15	6.155	6.439	0.284	6.472	0.317
17	6.398	6.357	−0.041	6.613	0.215
19	5.155	5.369	0.214	5.220	0.065
20	7.000	6.721	−0.279	6.248	−0.752
22	6.523	6.749	0.226	6.353	−0.170
23	5.398	5.623	0.225	5.947	0.550
24	6.699	6.875	0.176	6.903	0.204
25	6.000	6.114	0.114	6.051	0.051
26	5.699	5.683	−0.016	5.732	0.033
27	6.523	6.235	−0.288	6.260	−0.263
29	4.824	4.874	0.050	4.968	0.144
30	6.000	5.963	−0.037	5.950	−0.050
31	5.000	4.825	−0.175	4.746	−0.254
32	5.699	5.677	−0.022	5.570	−0.129
34	6.000	5.815	−0.185	5.731	−0.269
35	5.523	5.617	0.094	5.552	0.029
36	5.000	5.091	0.091	5.307	0.307
37	5.000	5.335	0.335	5.361	0.361
38	4.699	4.553	−0.146	4.716	0.017
40	6.523	6.361	−0.162	6.441	−0.082
41	5.301	5.329	0.028	5.103	−0.198
42	6.699	6.789	0.090	6.693	−0.006
44	6.523	6.339	−0.184	6.347	−0.176
45	6.699	6.492	−0.207	6.702	0.003
46	7.222	7.440	0.218	7.429	0.207
47	7.000	6.978	−0.022	7.420	0.420
49	8.097	8.231	0.134	7.755	−0.342
50	8.523	8.405	−0.117	8.321	−0.202
52	7.301	7.377	0.076	7.375	0.074
53	7.301	7.443	0.142	7.765	0.464
54	7.398	7.223	−0.175	7.656	0.258
55	7.301	7.628	0.327	7.376	0.075
56	7.699	7.318	−0.381	7.476	−0.223
58	6.699	6.831	0.132	6.378	−0.321
59	7.398	7.490	0.093	7.301	−0.097
60	8.000	7.993	−0.007	7.656	−0.344
61	7.523	7.445	−0.078	7.730	0.207
62	6.398	6.275	−0.123	6.481	0.083
63	7.097	6.990	−0.107	7.290	0.193
64	6.000	6.044	0.044	6.106	0.107
65	5.046	5.171	0.125	5.305	0.259
66	7.000	7.015	0.015	7.026	0.026
68	7.699	7.736	0.037	7.435	−0.264
Test set					
1	6.000	5.862	−0.138	5.500	−0.500
4	6.000	6.080	0.080	6.012	0.012
8	5.222	6.003	0.781	5.773	0.551
13	6.046	5.932	−0.113	6.102	0.056
16	6.523	6.499	−0.024	6.557	0.035
18	6.155	5.874	−0.281	6.121	−0.034
21	6.699	6.429	−0.270	6.360	−0.339
28	5.155	5.336	0.181	5.376	0.221
33	5.398	5.491	0.093	5.048	−0.350
39	5.000	5.344	0.344	5.418	0.418
(continued on next page)					

(continued on next page)

Table 4 (continued).

Compound	Observed pIC ₅₀	CoMFA		CoMSIA	
		Predicted	Residual	Predicted	Residual
43	6.699	6.489	−0.210	6.861	0.162
48	7.000	7.222	0.222	7.239	0.239
51	7.699	7.432	−0.267	7.131	−0.568
57	7.699	7.228	−0.471	7.125	−0.574
67	6.699	6.577	−0.122	6.099	−0.600
Average			−0.013		−0.085
Variance ^a			0.091		0.134

^a Population variance: RSS/n , for n compounds.

comparing the structures and activities of compounds 2–7, it can be found that the introduction of bulky R₁ substituents such as *tert*-butyl (compound 4), phenyl (compound 6) and 2-thienyl (compound 7) groups to 2-position of pyrimidine ring increases inhibitory activity, while small R₁ substituents in this region decrease activity. It can also be proved by the lower activity of the compounds 2 (R₁ = Me) and 3 (R₁ = Et). Three steric unfavorable yellow contours near the phenyl ring of compound 6 and 2-thienyl ring of compound 50, suggest that substituents on 2-thienyl or

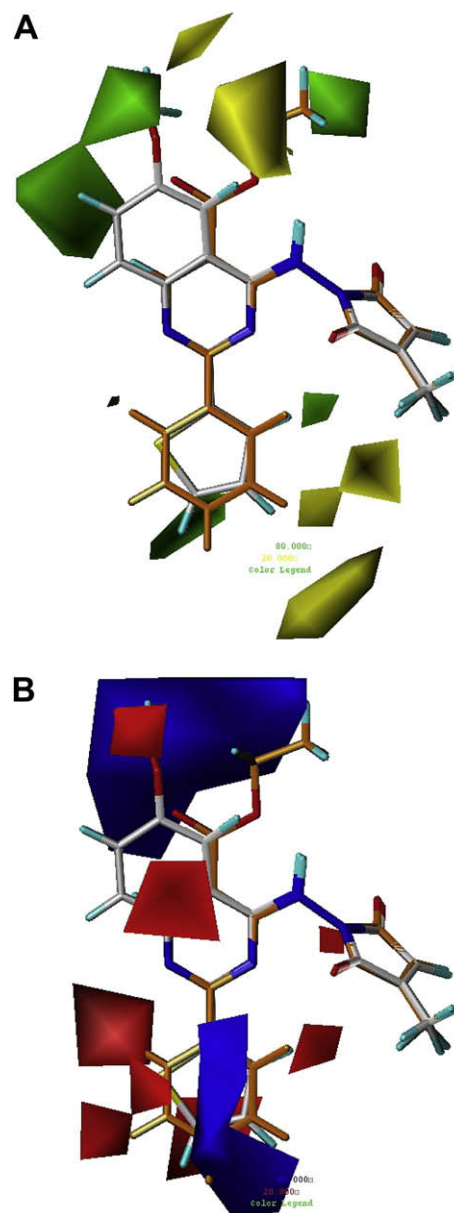


Fig. 4. CoMFA STDEV*COEFF contour maps based on compounds 6 (orange) and 50 (white): (A) steric fields: green contours (80% contribution) indicate regions where bulky groups increase activity, while yellow contours (20% contribution) indicate regions where bulky groups decrease activity, and (B) electrostatic fields: blue contours (80% contribution) indicate regions where electropositive groups increase activity, while red contours (20% contribution) indicate regions where electronegative groups increase activity (for interpretation of the references to colour in this figure legend, the reader is referred to the web version of this article).

phenyl ring falling into these regions would decrease activity. Moreover, in the CoMFA electrostatic contour map (Fig. 4B), a blue contour and a red contour are also distributed before and behind the 2-thienyl and phenyl planes indicating neither electropositive nor electronegative group here benefits activity. Therefore, these two contours and the three yellow regions discussed above can explain the fact that any substituent on phenyl or 2-thienyl ring in relevant compounds results in less inhibitory activity than their corresponding unsubstituted analogues [22]. For example, the introduction of Me (pIC₅₀ = 6.046), F (pIC₅₀ = 6.155), Cl (pIC₅₀ = 6.046) and CF₃ (pIC₅₀ = 6.389) to *meta*-position (compounds 13, 15, 16 and 17) and OMe (pIC₅₀ = 5.301), Br

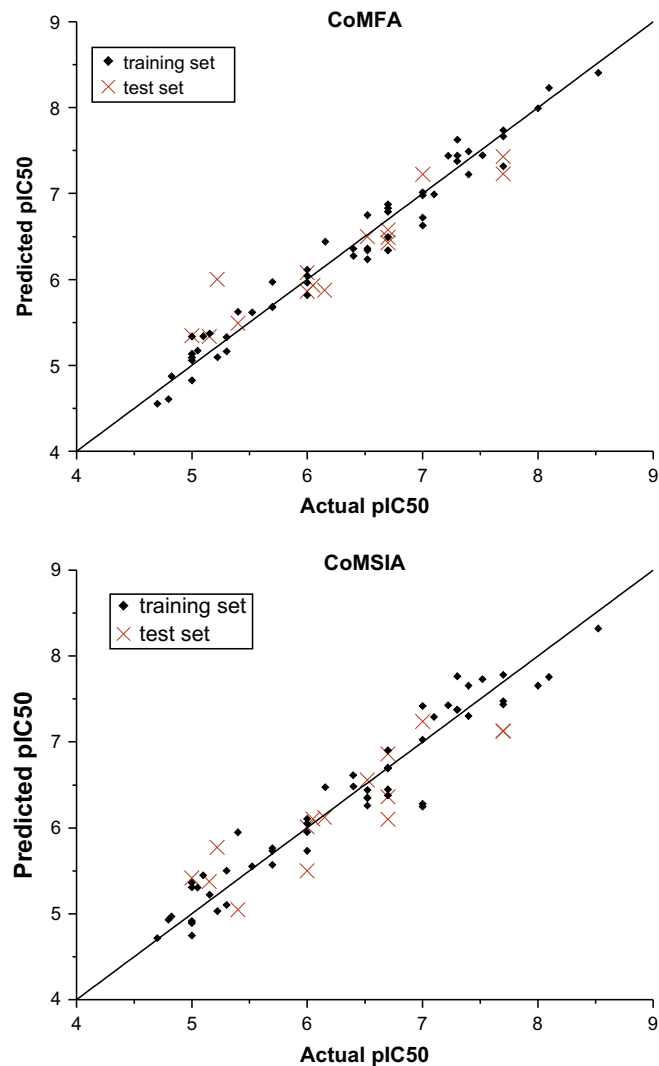


Fig. 3. Plot of the predicted versus observed pIC₅₀ values for all the molecules based on CoMFA ($q^2 = 0.594$, $r^2 = 0.968$) model (A) and CoMSIA ($q^2 = 0.703$, $r^2 = 0.932$) model (B).

($\text{pIC}_{50} = 6.155$) and NO_2 ($\text{pIC}_{50} = 5.155$) to *para*-position (compounds **14**, **18** and **19**) of phenyl ring gives lower activity than unsubstituted compound **6** ($\text{pIC}_{50} = 7.0$). Similarly, by comparing compound **7** ($\text{pIC}_{50} = 7.699$), 2-thienyl ring with Me ($\text{pIC}_{50} = 6.699$) or Cl ($\text{pIC}_{50} = 6.523$) group at 5-position (compounds **21** and **22**) decreases activities approximately to 1 logarithmic unit. The distribution of the yellow and green contours above and below the OEt moiety of compound **6** at top right corner in Fig. 4A indicates that the groups extending above can increase activity, while extending below can decrease activity. The OMe group at 6-position of quinazoline ring in compound **50** falling into a steric favorable green contour reveals the requirement of a R_6 substituent at this position. A small yellow steric unfavorable contour found near this green contour can also explain the fact that the higher activity can be obtained by medium-size steric bulky substituents such as OMe and Cl groups. In addition, a small red contour and a big blue contour are found near 6-position on quinazoline ring. This can explain the difference between the activities of the compounds **63** ($\text{pIC}_{50} = 7.097$), **64** ($\text{pIC}_{50} = 6.0$) and **65** ($\text{pIC}_{50} = 5.046$), with R_6 substituent of SMe, SOMe, and SO_2Me at 6-position, respectively, whose S atoms fall in the red contour and Me groups close to the blue contour. The green contour behind 7-position of quinazoline ring indicates the introduction of a fused phenyl on the pyrimidine ring (compounds **46–68**) that forms the quinazoline ring has a positive effect on inhibitory activity.

A cluster of three red contours appeared on the left side of R_1 substituent (Fig. 4B) shows that a electronegative group here is important to inhibitory activity, so compounds with R_1 substituent of 2-thienyl whose S atoms occupied this place gave higher activity than those with phenyl or CF_3 substituent. This can also

be demonstrated by the fact that compound **7** is more active than compounds **1** and **6**, while compound **46** is of higher potency than compounds **47** and **48**. The red contour before the phenyl moiety of quinazoline plane and the smaller one on the right side of R_1 substituent and behind 2-carbonyl oxygen on pyrrole ring suggest the favor of electronegative group at these regions.

3.3. CoMSIA contour maps

The contour map of all four fields (SEDA) for the best CoMSIA model is shown in Fig. 5, and the respective contour maps of the

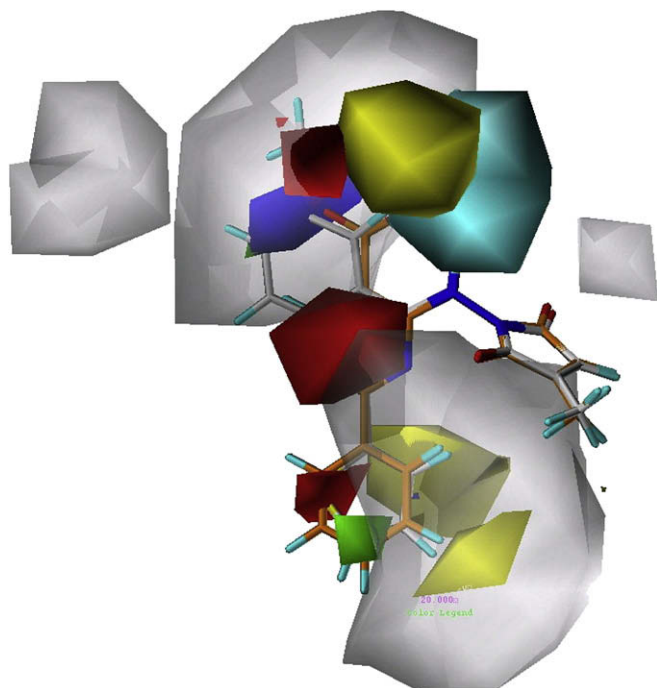


Fig. 5. CoMSIA STDEV*COEFF contour map of all four fields based on compounds **6** (orange) and **50** (white). Green and yellow (80% and 20% contributions) contours represent steric favorable and unfavorable regions, blue and red (80% and 20% contributions) contours depict sites favoring electropositive and electronegative groups, cyan and purple (not appeared) (80% and 20% contributions) contours indicate favorable and unfavorable H-bond donor groups, while white and magenta (80% and 20% contributions) contours depict favorable and unfavorable H-bond acceptor groups (for interpretation of the references to colour in this figure legend, the reader is referred to the web version of this article).

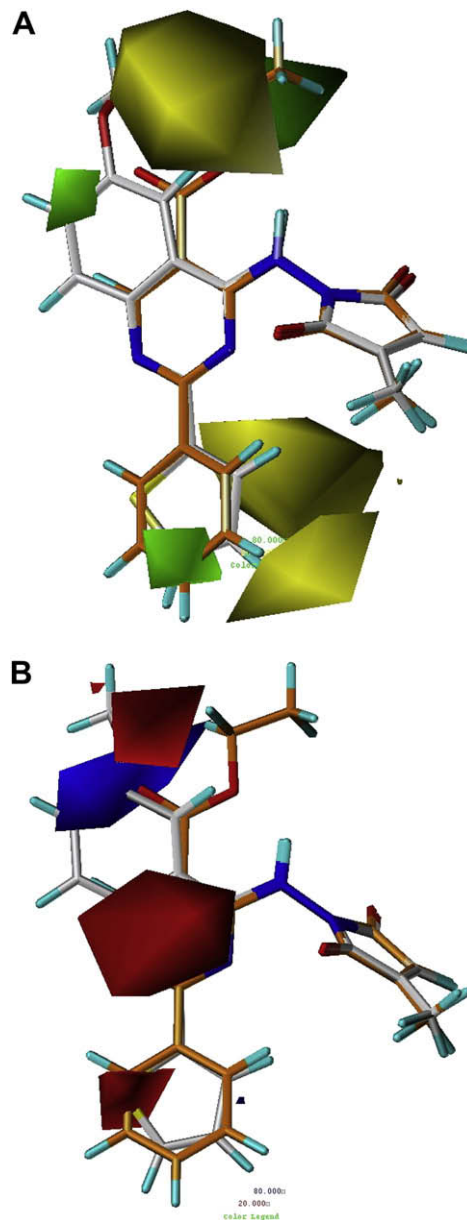


Fig. 6. CoMSIA STDEV*COEFF contour maps based on compounds **6** (orange) and **50** (white): (A) steric fields: green contours (80% contribution) indicate regions where bulky groups increase activity, while yellow contours (20% contribution) indicate regions where bulky groups decrease activity, and (B) electrostatic fields: blue contours (80% contribution) indicate regions where electropositive groups increase activity, while red contours (20% contribution) indicate regions where electronegative groups increase activity (for interpretation of the references to colour in this figure legend, the reader is referred to the web version of this article).

four CoMSIA fields are shown in Figs. 6 and 7. Fig. 6 shows steric and electrostatic contour maps while Fig. 7 shows hydrogen-bond fields maps. In Fig. 6, contours in green and yellow (80% and 20% contributions) represent steric favorable and unfavorable regions, blue and red (80% and 20% contributions) contours depict the sites favoring positively charged and negatively charged groups. It can be seen that the CoMSIA steric and electrostatic contour maps are very similar to the corresponding CoMFA contour maps. Moreover, in the contour map of CoMSIA, one yellow contour behind 2-thienyl of compound **50** and phenyl ring of compound **6** indicates that the occupancy of this region would decrease the inhibitory activity.

In Fig. 7, the cyan and purple (not appeared) (80% and 20% contributions) contours indicate favorable and unfavorable H-bond donor groups, respectively, while contours in white and magenta (80% and 20% contributions) depict favorable and unfavorable H-bond acceptor groups, respectively. One H-bonding donor feature, displayed by the cyan contour surrounding the NH linker at position of R_4 substituent in Fig. 7A, indicates that the NH linker

acts as H-bond donor and the replacement of this H atom will lead to lower activity. It can be proved by the fact that compounds **32**, **34** and **35** without H-bond donor at that position showed lower activity than their analogues **6**, **7** and **15** containing H-bond donor. Especially, compound **33** with Ac as R_4 substituent decreased inhibitory activity approximately to 1.6 logarithmic unit.

In Fig. 7B, the big white H-bond acceptor favorable contour around 3-N in quinazoline ring and 2-carbonyl oxygen on pyrrole ring, and the one near 4-carbonyl oxygen on pyrrole reveal that these atoms may act as H-bond acceptor. Another big white contour encompassing around phenyl moiety of quinazoline ring of R_6 shows that H-bond acceptor groups at 5, 6, 7 and 8 positions of quinazoline ring avail inhibitory activity. For instance, compounds with one or more OMe groups on quinazoline ring (compound **49–54** and **59**) resulted in higher inhibitory activity than compound **46** without R_6 substituent. Comparing activity of the compounds **60**, **61**, **63** and **68** with that of **48**, it also has the same trend. One small H-bond acceptor unfavorable magenta contour is encompassed by the white contour and behind carbonyl oxygen of CO_2Et group on pyrimidine ring of compound **6**, which suggests this O atom here is very important to the inhibitory activity. In summary, based on the results of the 3D-QSAR contour maps, more compounds with desired inhibitory activity could be obtained by further modification on the phenyl ring of the quinazoline ring of these compounds by considering the steric, electrostatic and hydrogen-bond acceptor features.

4. Conclusion

The 3D-QSAR models for 68 inhibitors of AP-1 and NF- κ B mediated transcriptional activation were developed using CoMFA and CoMSIA techniques. The best CoMFA and CoMSIA models gave the cross-validated q^2 values of 0.594 and 0.703, non-cross-validated r^2 values of 0.968 and 0.932, respectively. Based on the cross-validation results, it can be seen the CoMSIA model has better predictive ability than CoMFA model due to the importance of the hydrogen bonds for the activity of inhibitors. The CoMFA and CoMSIA contour maps can help to understand the structure–activity relationship and identify structural features influencing the inhibitory activity. Furthermore, the satisfactory predictive ability of 3D-QSAR models observed for the test set of compounds indicates that these models could be successfully used for predicting activity of the inhibitors and guiding the further modification of these compounds.

Acknowledgement

This work was supported by the Program for New Century Excellent Talents in University (No. NCET-07-0399).

References

- [1] A.M. Manning, A.J. Lewis, Rheumatoid Arthritis 1 (1997) 65–73.
- [2] A.M. Manning, Drug Discov. Today 1 (1996) 151–160.
- [3] C.S. Hill, R. Treisman, Cell 80 (1995) 199–211.
- [4] M. Karin, Curr. Opin. Cell Biol. 6 (1994) 415–424.
- [5] H. Sebban, G. Courtois, Biochem. Pharmacol. 72 (2006) 1153–1160.
- [6] M. Karin, Z.G. Liu, E. Zandi, Curr. Opin. Cell Biol. 9 (1997) 240–246.
- [7] P.A. Bauerle, T. Henkel, Annu. Rev. Immunol. 12 (1995) 141–179.
- [8] A.C.T.M. Vossen, H.F. Savelkoul, J. Mediat. Inflamm. 3 (1994) 403–408.
- [9] A.J. Lewis, Emerging Drugs: The Prospect for Improved Medicines, Annual Executive Briefing, vol. 31, Ashley Publication Ltd, 1996.
- [10] M.S.S. Palanki, A.M. Manning, Curr. Med. Chem. 9 (2002) 219–227.
- [11] T.J. Caggiano, A. Brazzale, D.M. Ho, C.M. Kraml, E. Trybulski, C.C. Chadwick, S. Chippari, L. Borges-Marcucci, A. Eckert, J.C. Keith, T. Kenney, D.C. Harnish, J. Med. Chem. 50 (2007) 5245–5248.
- [12] R.K. Sharma, S. Chopra, S.D. Sharma, V. Pande, M.J. Ramos, K. Meguro, J.i. Inoue, M. Otsuka, J. Med. Chem. 49 (2006) 3595–3601.
- [13] H.Z. Jin, B.Y. Hwang, H.S. Kim, J.H. Lee, Y.H. Kim, J.J. Lee, J. Nat. Prod. 65 (2002) 89–91.

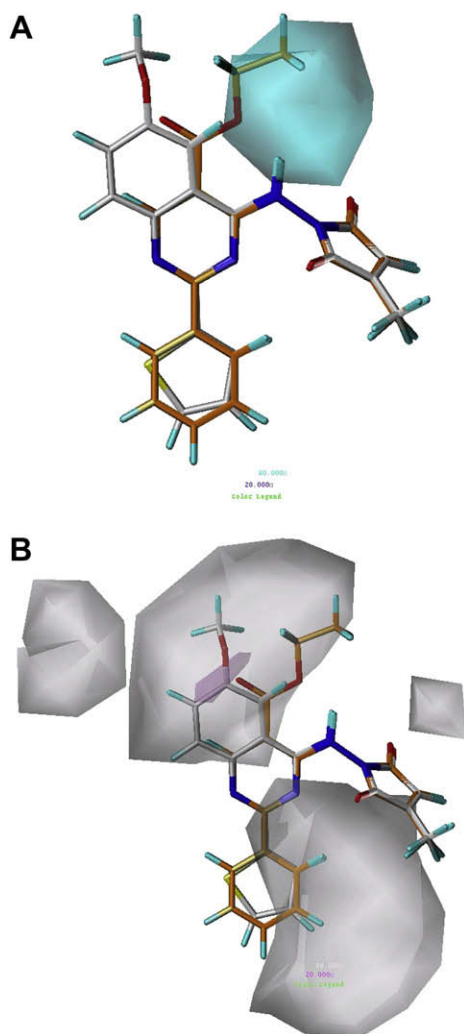


Fig. 7. CoMSIA STDEV*COEFF contour maps based on compounds **6** (orange) and **50** (white). (A) H-bond donor fields: cyan (80% contribution) and purple (20% contribution, which is not appeared) contours indicate hydrogen-bond donor groups favorable and unfavorable regions, respectively. (B) H-bond acceptor fields: white (80% contribution) and magenta (20% contribution) contours indicate regions where H-bond acceptor groups increase and decrease activity, respectively (for interpretation of the references to colour in this figure legend, the reader is referred to the web version of this article).

- [14] C. Li, E.A. Pace, M.C. Liang, E. Lobkovsky, T.D. Gilmore, J.A. Porco, J. Am. Chem. Soc. 123 (2001) 11308–11309.
- [15] K. Tsuchida, H. Chaki, T. Takakura, H. Kotsubo, T. Tanaka, Y. Aikawa, S. Shiozawa, S. Hirono, J. Med. Chem. 49 (2006) 80–91.
- [16] K. Tsuchida, H. Chaki, T. Takakura, J. Yokotani, Y. Aikawa, S. Shiozawa, H. Gouda, S. Hirono, J. Med. Chem. 47 (2004) 4239–4246.
- [17] G. Freire, C. Ocampo, N. Ilbawi, A.J. Griffin, M. Gupta, J. Mol. Cell. Cardiol. 43 (2007) 465–478.
- [18] R.W. Sullivan, C.G. Bigam, P.E. Erdman, M.S.S. Palanki, D.W. Anderson, M.E. Goldman, L.J. Ransone, M.J. Suto, J. Med. Chem. 41 (1998) 413–419.
- [19] M.S.S. Palanki, P.E. Erdman, L.M. Gayo-Fung, G.I. Shevlin, R.W. Sullivan, M.E. Goldman, L.J. Ransone, B.L. Bennett, A.M. Manning, M.J. Suto, J. Med. Chem. 43 (2000) 3995–4004.
- [20] M.S.S. Palanki, L.M. Gayo-Fung, G.I. Shevlin, P. Erdman, M. Sato, M. Goldman, L.J. Ransone, C. Spooner, Bioorg. Med. Chem. Lett. 12 (2002) 2573–2577.
- [21] M.S.S. Palanki, P.E. Erdman, A.M. Manning, A. Ow, L.J. Ransone, C. Spooner, C. Suto, M. Suto, Bioorg. Med. Chem. Lett. 10 (2000) 1645–1648.
- [22] M.S.S. Palanki, P.E. Erdman, M. Ren, M. Suto, B.L. Bennett, A. Manning, L. Ransone, C. Spooner, S. Desai, A. Ow, R. Totsuka, P. Tsao, W. Toriumi, Bioorg. Med. Chem. Lett. 13 (2003) 4077–4080.
- [23] Annals New York Academy of Sciences 766 (1995) 245–252.
- [24] R.D. Cramer III, D.E. Patterson, J.D. Bunce, J. Am. Chem. Soc. 110 (1988) 5959–5967.
- [25] G. Klebe, U. Abraham, T. Mietzner, J. Med. Chem. 37 (1994) 4130–4146.
- [26] M. Bohm, J. Sturzebecher, G. Klebe, J. Med. Chem. 42 (1999) 458–477.
- [27] A.V. Raichurkar, V.M. Kulkarni, J. Med. Chem. 46 (2003) 4419–4427.
- [28] D.S. Puntambekar, R. Giridhar, M.R. Yadav, Eur. J. Med. Chem. 43 (2008) 142–154.
- [29] N. Nunthaboot, S. Tonmuphean, V. Parasuk, P. Wolschann, S. Kokpol, Eur. J. Med. Chem. 41 (2006) 1359–1372.
- [30] Sybyl version 6.9, Tripos Associates, St. Louis (MO), 2001.
- [31] M. Clark, R.D. Cramer III, N.V. Opdenbosch, J. Comput. Chem. 10 (1989) 982–1012.
- [32] J. Gasteiger, M. Marsili, Tetrahedron 36 (1980) 3219–3228.
- [33] V.N. Viswanadhan, A.K. Ghose, G.R. Revankar, R.K. Robins, J. Chem. Inf. Comput. Sci. 29 (1989) 163–172.
- [34] G. Klebe, J. Mol. Biol. 237 (1994) 212–235.
- [35] G. Klebe, T. Mietzner, F. Weber, J. Comput. Aided Mol. Des. 13 (1999) 35–49.
- [36] S. Wold, C. Albano, W.J. Dunn, U. Edlund, K. Esbenson, P. Geladi, S. Hellberg, W. Lindburg, M. Sjostrom, in: B. Kowalski (Ed.), Chemometrics: Mathematics and Statistics in Chemistry, Reidel Dordrecht, The Netherlands, 1984, pp. 17–95.
- [37] L. Stahle, S. Wold, J. Chemom. 1 (1987) 185–196.
- [38] S. Wold, Technometrics 20 (1978) 397–405.
- [39] G. Bringmann, C. Rummey, J. Chem. Inf. Comput. Sci. 43 (2003) 304–316.